ELSEVIER

Journal of Non-Crystalline Solids 274 (2000) 364–372

JOURNAL OF NON-CRYSTALLINE SOLIDS

www.elsevier.com/locate/jnoncrysol

Section 22. Computer simulation II

Interplay between electronic and atomic structure in expanded fluid potassium: a path-integral molecular dynamics study

P.A. Deymier [a,*], Ki-Dong Oh [b]

[a] *Department of Materials Science and Engineering, University of Arizona, 1235 N. Campus Drive, Tucson AZ 85721-0012, USA*
[b] *Department of Physics, University of Arizona, 1235 N. Campus Drive, Tucson AZ 85721-0012, USA*

Abstract

The interplay between the electronic and atomic structure is studied for expanded supercritical fluid potassium using the method of path integral molecular dynamics. Upon expansion of liquid potassium, a transition occurs at nearly two times the critical density. As density decreases to that density, the fluid retains the properties of a metal with electron correlation enhancing its kinetic energy relative to the free electron gas. The calculated enhancement in kinetic energy is described adequately by the Hubbard model. As density and atomic coordination decrease, there is evidence for the formation of diamagnetic spin-paired electronic species. The computer simulation results are shown to be in good qualitative agreement with available experimental data for another alkali fluid, namely cesium. © 2000 Elsevier Science B.V. All rights reserved.

PACS: 71.30+h; 71.15.Pd; 71.27.+a; 71.22.+i

1. Introduction

While the electronic structure of crystalline metal is well understood, much less is known about non-crystalline metals. The lack of periodicity in non-crystalline metals renders the description of their electronic structure difficult. In this paper, we investigate the electronic structure of a simple non-crystalline metal, namely a liquid alkali metal. The correlation between the structure of a liquid metal and its electronic structure is best exemplified by the observation of a metal/insulator (M/I) transition at the critical point density in thermally expanded alkali fluid [1]. As density decreases, so does electrical conductivity [1]. In a density range near the critical density, the conductivity decreases sharply below the minimum metallic conductivity of 10^2 Ohm^{-1} cm^{-1} where semiconducting behavior takes place [1]. The M/I transition has also been detected by measuring the magnetic susceptibility or the Knight shift in nuclear magnetic resonance (NMR) experiments. Measurements of the paramagnetic susceptibility of fluid alkali metals have been conducted by Freyland [2]. In expanded Cs liquid, the paramagnetic susceptibility initially decreases with decreasing density to approximately 3/4 of the density at the melting point or three times the critical density (see Fig. 1(a)). The

* Corresponding author. Tel.: +1-520 621 6080; fax: +1-520 621 8059.
E-mail address: deymier@oxygen.mse.arizona.edu (P.A. Deymier).

0022-3093/00/$ - see front matter
PII: S0022-3093(00)00196-4

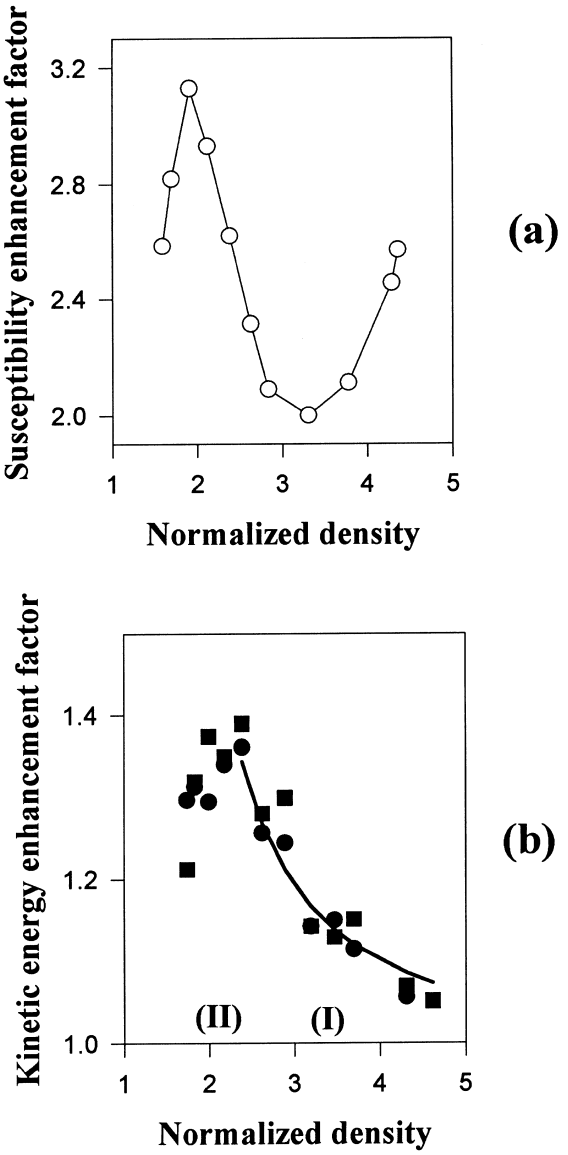

Fig. 1. (a) Experimental paramagnetic susceptibility enhancement factor of fluid Cs versus density normalized to the critical density (from Ref. [2]), (b) Electron kinetic energy enhancement factor of liquid potassium versus density normalized to the critical density. The circles and squares are calculated with the estimators of Refs. [16] and [17], respectively. I and II refer to the high and low density regions. The solid line is a fit to the data in the high-density region (see text for details).

decrease in susceptibility is then followed by an increase with further expansion. A maximum is observed at a density of approximately 0.44 times the density at the melting point or two times the critical density. At even smaller density, on the vapor side, the susceptibility increases with decreasing density, yielding an apparent minimum near the critical point. The Knight shift was measured by Warren and Brennert in NMR experiment [3]. From the measurements of the Knight shift of Cs, one could extract the Fermi-level electron density at the nucleus. The charge density at the nucleus exhibits a decrease with decreasing density in the range 0.44–0.77 times the density at the melting point.

Mott [4] has stressed the importance of electron correlation in the M/I transition and the Mott transition has been called upon to explain some features of expanded alkali fluids. For instance, let us consider the expansion of a perfect lattice of one-electron atoms within the Hubbard model including only the intra-atomic electron correlation. On a lattice, the competition between the electron kinetic energy (quantified by an overlaping energy integral such as in the tight binding model with band width B) and the intra-atomic energy of two electrons on a given site (U) may open a gap in the electronic energy spectrum leading to the formation of the so-called lower and upper Hubbard bands. At small intra-atomic energies compared to the band width, the Hubbard bands overlap and the system is similar to a paramagnetic metal. For large U/B, the system has the properties of an insulator. There is also the possibility of antiferromagnetic order in the insulating state. It has often been suggested that the Hubbard model may then be the relevant Hamiltonian for expanded alkali fluids. Brinkman and Rice [5] have shown that the Hubbard model with intra-atomic Coulomb interaction predicts an enhancement of the magnetic susceptibility relative to the free electron gas as the M/I transition is approached from the metal side. Lattice-based electronic models predict that the electron density at the nucleus should increase as the density (or coordination) decreases in contradiction with the results of the experimental work of Warren and Brennert [3].

More recently, models of expanded alkali fluids have recognized the importance of clusters, in particular at low density. Redner and Warren [6]

have proposed a model of partially ionized gas in support of cluster formation. They calculate the electronic magnetic susceptibility of Cs and Rb from the vapor to the liquid phase. The deviations from the Curie law on the vapor side are due to the formation of spin-paired dimers. In this model increase of the susceptibility at around two times the critical density in the regime of the expanded liquid can be explained by the formation of Cs_2^+ and Rb_2^+. The idea that there is cluster formation in the expanded alkalis has also been discussed by Hernandez [7]. Reverse Monte Carlo modeling of the structure factor of expanded cesium has shown that as density decreases clustering takes place and that the metal–non-metal transition may be thought of as a bond percolation transition [8].

In this paper, we present a computer simulation study of the electronic structure and atomic structure of an expanded supercritical potassium fluid. Computer simulations have the advantage of providing under controlled conditions a multitude of quantities not accessible to experiment. These simulations allow us to show the interplay between atomic and electronic structure in fluid metals.

2. Method and models

We employ a recently developed first-principle molecular dynamics method applicable to the simulation of interacting many-fermion systems at finite temperature: the restricted path integral molecular dynamics (PIMD) method [9,10]. This method makes use of (a) the discretized path integral representation of quantum particles as closed chains (or necklaces) of P classical particles (beads) with quantum exchange treated through cross-linking of the chains [11], (b) the non-locality of cross-linking along the chains [12,13], (c) the restricted path integral [14]. The combination of these three parts results in a classical effective potential for the representation of indistinguishable quantum particles.

The PIMD method models an assembly of fermions (electrons) and ions with the classical Hamiltonian [10,15]:

$$
\begin{aligned}
H = & \sum_{k=1}^{Nel}\sum_{i=1}^{P}\frac{1}{2}m^*\left(\dot{r}_i^{(k)}\right)^2 + \sum_{I=1}^{Nion}\frac{1}{2}M_I\dot{R}_I^2 \\
& + \sum_{I>J}^{Nion}\sum_{I=1}^{Nion-1}\Phi_{IJ}(R_{IJ}) \\
& + \sum_{i=1}^{P}\sum_{k>l}^{Nel}\sum_{l=1}^{Nel-1}\frac{(-e)(-e/P)}{4\pi\varepsilon_0\left|r_i^{(k)}-r_i^{(l)}\right|} \\
& + \sum_{i=1}^{P}\sum_{k=1}^{Nel}\sum_{I=1}^{Nion}\frac{V_{\text{pseudo}}\left(R_I-r_i^{(k)}\right)}{P} \\
& + \sum_{k=1}^{Nel}\sum_{i=1}^{P}{}^{*}\frac{m_eP}{2\hbar^2\beta^2}\left(r_i^{(k)}-r_{i+1}^{(k)}\right)^2 \\
& - \frac{1}{\beta}\sum_{s=\uparrow}^{\downarrow}\frac{\sum_{i=1}^{P}\sum_{j=1}^{P}\ln\det\left[E_{ij}\right]_s\theta_{ijs}^{+}}{\sum_{i=1}^{P}\sum_{j=1}^{P}\theta_{ijs}^{+}}.
\end{aligned}
\tag{1}
$$

Here, m^* is an arbitrary mass (we chose $m^* = 1$ a.u.) defining an artificial kinetic energy for the electron necklace beads. The second term is the kinetic energy of the ions. The position of the electron beads and the ions is indicated by r and R, respectively. The ion interactions are represented by a long range Coulomb repulsion and a short range Born–Mayer potential, both included in Φ_{IJ} [15]. The fourth term accounts for the electron Coulomb interactions. The ion/electron potential is denoted V_{pseudo} and we use an empty core local pseudopotential with a core radius $R_c = 2.22$ Å [15]. The sixth term is the effective harmonic potential for distinguishable quantum particles. The cyclic condition on the summations over the beads is denoted by a '*'. Finally, the seventh term is an exchange potential for the electrons with identical spin $s = \uparrow$ or $\downarrow$. The function θ_{ij}^{+} ensures a restriction on the paths [14] by taking on the values 1 and 0 for paths with positive and negative $\det[E_{ij}]$. The exchange effects (i.e. permutations between identical particles) are included in the matrix $[E_{ij}]$ which elements are defined as $E_{ij}^{kl} = A_{ij}^{kl}/A_{ij}^{kk}$ with

$$
A_{ij}^{kl} = \exp\left(-\frac{m_eP}{2\beta\hbar^2}\left(r_i^{(k)}-r_j^{(l)}\right)^2\right)
$$

where k and l label the electrons. The indices i and j label beads along necklaces. The term $\det[E_{ij}]_s$

includes all the permutations between electrons with identical spin s. It is this term that leads to electrons distributing according to Fermi statistics. M_I and m_e stand for the ion and electron masses and $\beta = 1/k_B T$. We employ periodic boundary conditions (PBC) in a manner similar to that of reference [15].

We study a fluid system that contains 30 potassium atoms. One-half of the 30 valence electrons have a spin up, the other half having a spin down. The long range Coulomb potentials are replaced by a shorter-range potential of the form $1/r \to (1/r)\mathrm{erfc}(\eta r)$ where $\eta = 5.741/L_0$ and $L_0 = 13.3$ Å. erfc stands for the complementary error function. All potentials are truncated at half the size of the edge of the simulation box.

We solve the equations of motion with a leap frog scheme and an integration time step of 2.1×10^{-16} s. Most simulations of the liquid metal lasted at least 15 000 time steps but the simulations for which structural information is reported lasted up to 45 000 steps. The simulations are run sequentially from high to low density, using an equilibrated configuration from one simulation as starting configuration for the next one. We rescale the temperature of each electron necklace independently of each other and of the ions via a momentum rescaling thermostat. We set the temperature of the ions in the fluids to the experimental critical temperature of 2220 K [16]. The PIMD does not permit the simulation of electrons at very low density and very high temperature (such as the critical temperature) [15], the electrons are therefore maintained at the lower temperature of 1300 K. At this temperature and the densities studied, the electrons are nearly degenerate and temperature should have little impact on electronic properties. We use $P = 300$ beads for each electron necklace. This choice is made to ensure convergence of the path integral at the temperatures and densities studied [10]. For all simulations, we calculate the kinetic energy with the energy estimator of Ref. [17]. Since some of the simulations of the small fluid last only 15 000 steps, we also calculate the kinetic energy with a second estimator [18]. We, therefore, estimate the error on the kinetic energy of the electrons to be on the order of 0.05 eV.

3. Results and discussion

In Fig. 1(b) we report the calculated kinetic enhancement factor of the expanded liquid potassium as a function of density normalized to the critical density. The kinetic energy enhancement factor is defined as the ratio of the kinetic energy of the system and the kinetic energy of free electrons. For comparison, we also show the experimental paramagnetic susceptibility enhancement factor (ratio of the susceptibility to that of a free electron) versus normalized density for another alkali metal, namely Cs [2].

The calculated kinetic energy enhancement factor has two dependencies. From a normalized density of 4.5 to approximately 2 (subsequently called region I) the kinetic energy enhancement factor increases followed by a decrease for densities <2 (region II). The maximum in the calculated kinetic energy enhancement factor near a normalized density of 2 is in agreement with that of the measured susceptibility enhancement factor. Whereas the calculated kinetic energy and measured susceptibilities vary differently in the vicinity of the density at melting. Freyland has interpreted the increase in the paramagnetic susceptibility at the density of the melting point in terms of the Stoner model [4]. The decrease in susceptibility from one to approximately 3/4 the density at the melting point was explained by a reduction in the exchange-correlation integral with increasing expansion. Since the susceptibility enhancement factor predicted by the Stoner model is not associated with an enhancement in the electron effective mass (or kinetic energy) relative to the free electron gas. The simulation results are, therefore, not in contradiction with the experiment. Freyland [2] has argued that the subsequent increase in the magnetic susceptibility enhancement factor he observed in expanded liquid Cs down to two times the critical density detected the dramatic paramagnetic enhancement explored by Brickman and Rice [5]. Brinkman–Rice's model predicts in addition to an increase in susceptibility an increase in effective mass. Such an increase would result from a decrease of the electronic bandwidth as one reduces the atomic density and atomic coordination.

Fig. 2 reports the ion pair distributions, $g_{KK}(r)$, for two densities characteristic of the fluid metal in regions I and II. The greater-density fluid has a first nearest neighbor peak at approximately 4.1 Å. Note that it is not possible to extract information for distances exceeding one half the length of the edge of the simulation cell. This radial distribution function is characteristic of the normal metal fluid. It compares relatively well with experimental data. An experimental ion pair distribution of liquid potassium near the melting point ($T_m = 333$ K) shows a first nearest neighbor peak at approximately 4.5 Å, a minimum near 6.5 Å and a second nearest neighbor maximum at 8.6 Å [19]. The softer first nearest neighbor peak of our model results from larger ion displacements owing to the high temperature as well as the weaker coulomb interactions. As density decreases from region I to region II, the first nearest neighbor peak broadens and the ion correlation peaks near 4.5 Å. This change is indicative of a reduced coordination number and a smearing out of the fluid structure. The ionic structure in region II may then be visualized as a liquid with defects. Overall, the persistence of the first nearest neighbor distance around 4–4.5 Å over the entire range of density is evidence for a tendency in the expanded fluid to maintain bonding.

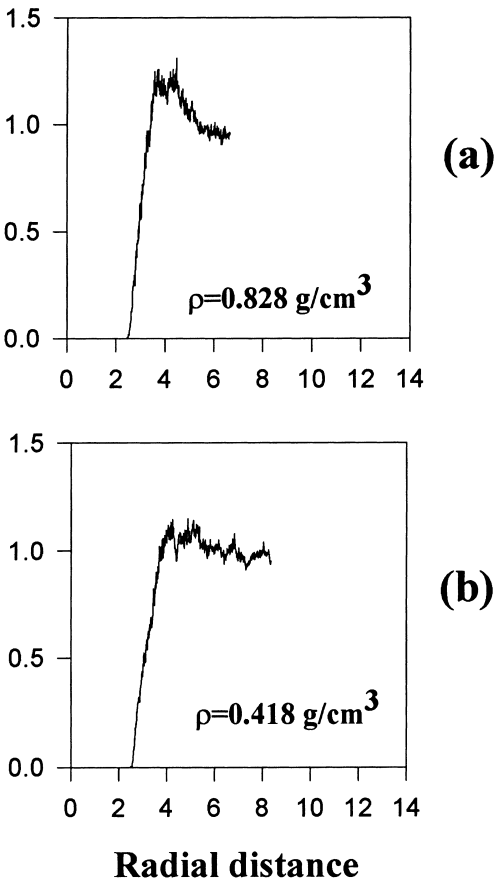

Fig. 2. Ion pair distributions at: (a) high density and (b) low density. The densities are indicated in the figure. The radial distance is in Å.

We have calculated the average coordination number by integration of $\rho g_{KK}(r)4\pi r^2\,dr$ up to a cut off radius of 6 Å. The average coordination number as a function of density is presented in Fig. 3. The average coordination number decreases linearly as density decreases. The coordination number is estimated by the approximate relation $Z = 14\rho$, where ρ is the mass density given in g/cm^3. This calculated linear evolution is in agreement with the reverse Monte Carlo analysis of the experimental structure factor of expanded cesium along its liquid–vapor coexistence curve [8] as well as Freyland's results of neutron diffraction experiments on expanded fluid rubidium cited in

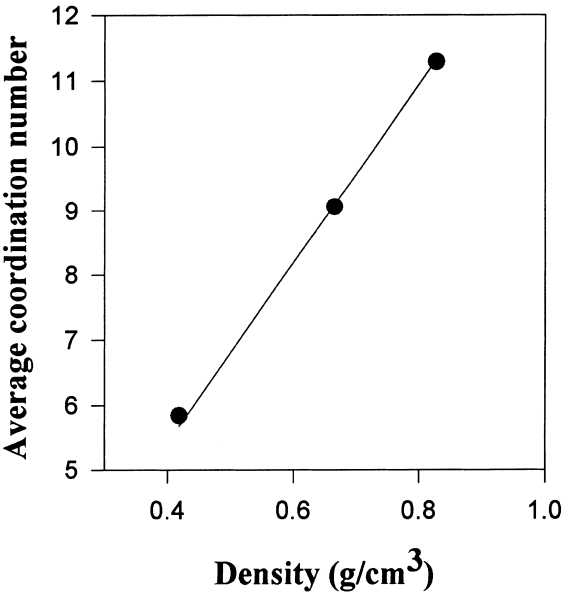

Fig. 3. Calculated average coordination number as a function of density. The line is a fit of a linear function to the data.

[2]. At larger densities, ions in the fluid are strongly coordinated with a coordination number between 11 and 12. In the body-centered cubic structure of crystalline potassium, atoms are surrounded by eight first-nearest neighbors and six second-nearest neighbors. In the larger-density liquid, the distinction between first- and second-nearest neighbors is lost and the coordination number approaches 14. As the fluid expands, the decrease in coordination can be described by a defected liquid with an increasing number of 'vacancies'. The transition between regions I and II occurs near an average coordination number of 6. Analysis of individual structures indicates that the distribution of coordination numbers extends from approximately 8 to 15 and from 1 to 9 at the largest and smallest densities studied, respectively.

To get a semiquantitative description of the kinetic energy enhancement factor in region I in terms of structural factors, we use the Brinkman–Rice model of a strongly correlated metal. Following Brinkman and Rice [5], the kinetic energy enhancement factor as a function of density should take the functional form: $f(\rho) = (1 - (U/C_0(\rho))^2)^{-1}$, where U represents the Hubbard intra-atomic energy (i.e. energy of two electrons on one atomic site) and C_0 is 8 times the modulus of the average energy without correlation. Mott [4] estimated C_0 to be on the order of the bandwidth, B. We estimate the bandwidth by $B = 2ZI$, where I is the overlap energy integral. In the range of densities studied, we use: $Z = 14\rho$. We rewrite the enhancement factor in the form: $f(\rho) = (1 - (a/\rho)^2)^{-1}$, where $U/28I = a$ and the density, ρ, is in units of g/cm^3. The overlap energy integral, I, can be estimated as the kinetic energy, $I = \hbar^2/2md^2$, where d is the interatomic distance. On the basis of the ion pair correlation functions, we chose for our model $d \sim 4.5$ Å, the distance an electron would have to hop as it goes from one ion to a neighboring one. We therefore obtain an overlap energy integral of 0.187 eV. The intra-atomic energy corresponds to the Coulomb energy of two heterospin electrons on one atomic site. In our model, the Coulomb interaction is replaced by a shorter-range potential of the form: $(1/r)$ erfc(ηr), where $\eta = 5.741/13.3$. Two-electrons in the same ion core are expected to be separated by a distance approximately equal to the core radius of 2.22 Å, thus giving $U \sim 1.16$ eV. From the estimated overlap energy integral and the intra-atomic energy, we obtain an estimate $a \sim 0.22$ g/cm^3. As a check, we have fitted the function of density, $f(\rho) = (1 - (a/\rho)^2)^{-1}$, to the calculated kinetic energy enhancement factor (see the solid line in Fig. 1). A least square fit is obtained for $a = 0.232$ g/cm^3. Owing to the estimates of U and I, the estimated parameter a is in accord with the a obtained from the fit to the kinetic energy enhancement factor.

The evolution of the correlated electronic structure with decreasing density is best seen in the electron pair distributions in Fig. 4. The heterospin electron pair distributions, $g_{\uparrow\downarrow}$, account for contributions from electron–electron interactions. $g_{\uparrow\downarrow}$ ought not vanish at $r = 0$. The sudden decrease in isospin electron pair distributions toward zero for distances shorter than 0.3 Å results from the finite P and constitutes a limitation of the PIMD method. The isospin electron pair distributions, $g_{\uparrow\uparrow \text{and} \downarrow\downarrow}$, account for exchange effect in addition to the electron–electron interaction. As density varies from regions I to II the correlation between heterospin electrons decreases only slightly for distances in the interval [2,4 Å]. In contrast, the

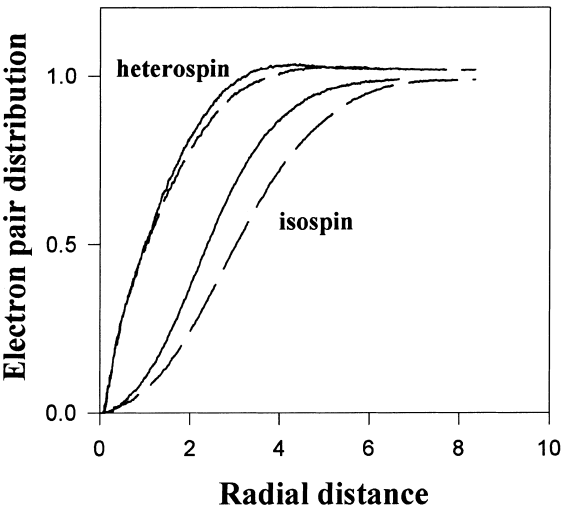

Fig. 4. Partial electron pair distributions. The solid line and dashed lines correspond to a high-density and a low-density fluid, respectively (see Fig. 2 for density values). The radial distance is in Å.

exchange-correlation hole between isospin electrons is enlarged. We suggest that these electron pair distributions, as density decreases, evolve toward those of spin-paired electronic species.

We also consider the partial electron–ion radial distributions in Fig. 5. Over long time periods of our simulations, the average radial distributions of spin-up, $g_{\uparrow I}(r)$ and spin-down, $g_{\downarrow I}(r)$ electrons about the ions converge to a same form. For all densities studied, the electron density is largest at approximately 2.2 Å from the ion. This distance corresponds to the edge of the ion core and indicates that the electrons are shared by neighboring ions and therefore participate in bonding. There is also some long-range correlation in the electron–ion distribution complementary to the ion pair correlation, namely a minimum near 4 Å and a weak maximum near 6 Å.

We have used the partial electron–ion radial distributions to calculate the partial average electron number density in a shell of radius, r, and thickness, $dr = 0.01$ Å. The partial average electron number density is given as: $n(r)\,dr = N_s/Vg_{sI}(r)4\pi r^2\,dr$, where N_s is the number of electrons with spin 's' in the simulation cell of volume, V. Fig. 6 shows that the electron wave function spreads as atomic density decreases. The extent of electron 'delocalization' may then be quantified by the electron radius, R_e, defined as $\int_0^{R_e} n(r)\,dr = 1$. The electron radius ranges from $R_e \sim 2.6$ to 3.3 Å for the largest and smallest density systems considered here. Our calculation of an electron wave function spreading out as atomic density decreases is consistent, in particular in region I, with the experimental observation of Warren and Brennert of a substantial reduction in electron charge density at the nucleus [3].

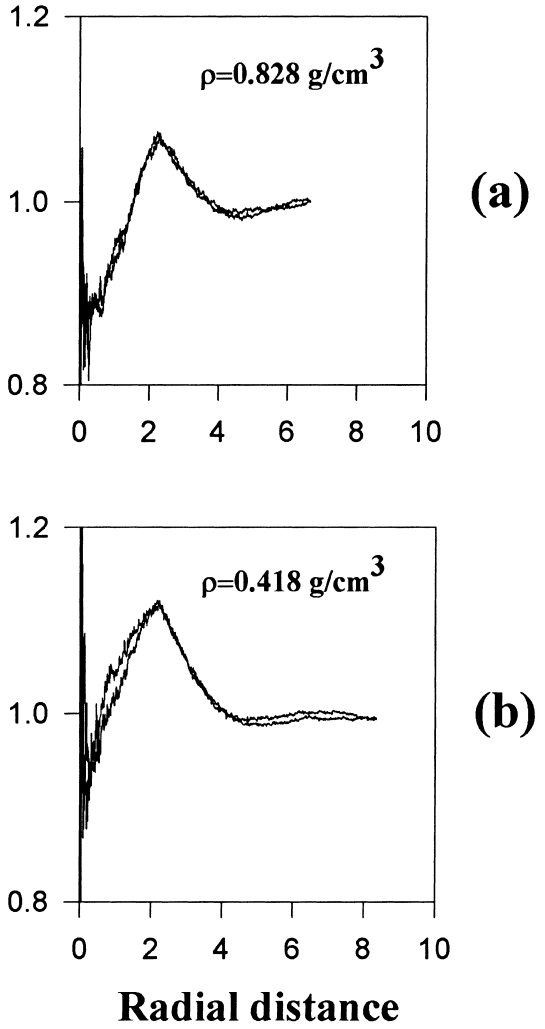

Fig. 5. Up-spin and down-spin electron–ion radial distributions for (a) high-density fluid and (b) low-density fluid. The radial distance is in Å.

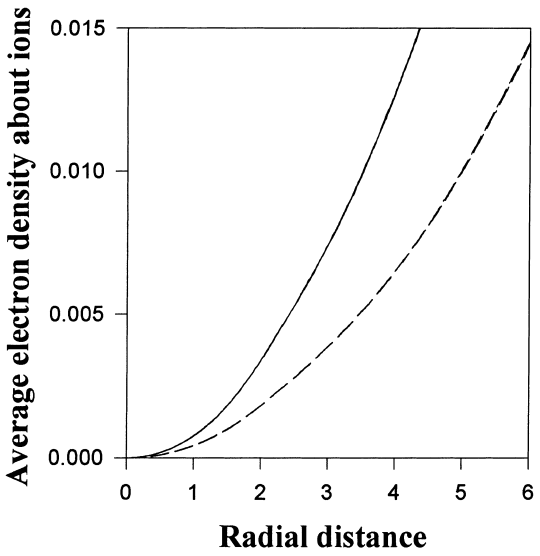

Fig. 6. Average partial electron number density about ions. The solid line and dashed lines correspond to a high-density and a low-density fluid, respectively. The radial distance is in Å.

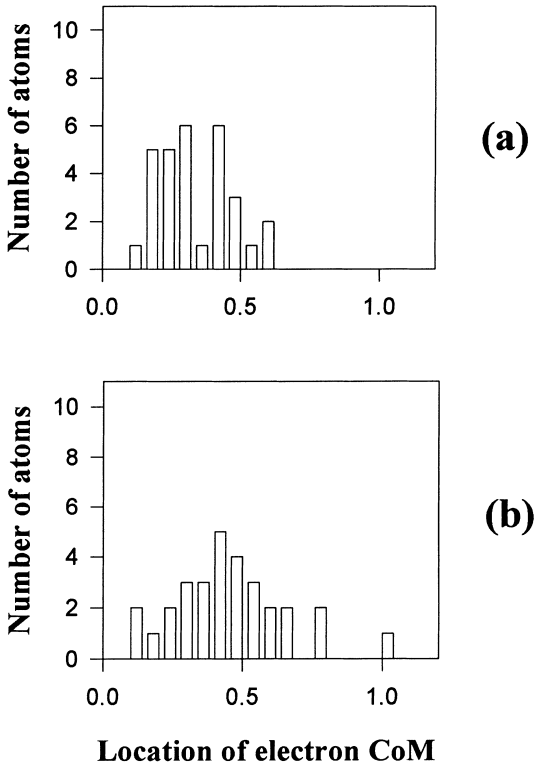

Fig. 7. Distribution of the location of the electron center of mass from the ion center (in Å) for (a) a high density fluid and (b) a low-density fluid.

By definition, electron–ion radial distributions do not provide information concerning the symmetry of the electron density around an ion. To remedy this deficiency, we have calculated the location of the center of mass of the electron cloud about every ion. This calculation uses instantaneous equilibrated electron/ion configurations. The center of mass is calculated as the sum of the position of all electron beads within the electron radius, R_e, of every ion. Fig. 7 reports the distribution of the distance of the electron center-of-mass from every ion for two densities. As density decreases, the distribution of centers of mass broadens. The two observations that: (a) the centers of mass are nearly centered on the ion core and (b) the electron–ion radial distribution peaks at 2.2 Å, suggest that at high atomic density, the electrons take on a spherically symmetric form reminiscent of a '*s*-type' wave function. With increasing 'delocalization' of the electrons within the ion cores, the degree of asymmetry in the electron density about the ions increases. The reduced atomic coordination in the fluid at low-density does not allow the wave function to maintain its '*s*' character, that is, with smaller atomic coordination, the spherical symmetry of atomic arrangement is gradually lost. Below two times the critical density, some atoms have very low coordination (i.e. 1, 2 or 3), the electronic structure evolves toward molecular orbitals. This evolution toward spin paired diamagnetic species can therefore explain the decrease in the paramagnetic susceptibility (or kinetic energy) enhancement factor in density region II.

4. Conclusions

In conclusion, this study shows the interplay between atomic and electronic structure in non-crystalline metals. It stresses the weakness of computer simulations based on empirical potentials in the study of amorphous metals and demonstrates the need to use first-principle-based methods that include correlation between electronic and atomic structures.

References

[1] W.W. Warren Jr., in: P.P. Edwards, C.N. Rao (Eds.), The Metallic and Non-metallic States of Matter, Taylor and Francis, London, 1985.
[2] W. Freyland, Phys. Rev. B 20 (1979) 5104.
[3] W.W. Warren Jr., G.F. Brennert, Phys. Rev. B 39 (1989) 4038.
[4] N.F. Mott, Metal–Insulator Transitions, Taylor and Francis, London, 1974.
[5] W.F. Brinkman, T.M. Rice, Phys. Rev. B 2 (1970) 4302.
[6] R. Redner, W.W. Warren, Phys. Rev. B 48 (1993) 14892.
[7] J.P. Hernandez, Phys. Rev. Lett. 57 (1986) 3183.
[8] V.M. Nield, M.A. Howe, R.L. McGreevy, J. Phys. 3 (1991) 7519.
[9] K.-D. Oh, P.A. Deymier, Phys. Rev. B 58 (1998) 7577.
[10] K.-D. Oh, P.A. Deymier, Phys. Rev. Lett. 81 (1998) 3104.
[11] D. Chandler, P. Wolynes, J. Chem. Phys. 74 (1981) 4078.
[12] R.W. Hall, J. Chem. Phys. 89 (1988) 4212.
[13] R.W. Hall, J. Chem. Phys. 91 (1989) 1926.

[14] D.M. Ceperley, J. Stat. Phys. 63 (1991) 1237.
[15] K.-D. Oh, P.A. Deymier, Phys. Rev. B 59 (1999) 11276.
[16] R.W. Ohse, Handbook of Thermodynamic and Transport Properties of Alkali Metals, Blackwell, Oxford, 1985.
[17] J.A. Barker, J. Chem. Phys. 70 (1979) 2914.
[18] M.F. Herman, E.J. Bruskin, B.J. Berne, J. Chem. Phys. 76 (1982) 10.
[19] Y. Waseda, in: The structure of Non-crystalline Materials, McGraw Hill, New York, 1980.